Journal of Ceramic Processing Research. Vol. 9, No. 1, pp. 52~56 (2008)

J O U R N A L O F
Ceramic Processing Research

Electrochemical characteristics of Tin-based anode material for Li-ion secondary batteries

Jangwon Oh[a], Kihyun Cho[a], Taewon Lee[a], Insoo Hwang[a], Siyoul Jang[b] and Dongwook Shin[a,*]

[a]*Division of Materials Science and Engineering, Hanyang University, 17 Haengdang-dong, Seongdong-gu, Seoul, 133-791, Korea*
[b]*School of Mechanical and Automotive Engineering, Kookmin University, Korea*

Recently tin-based composite oxide materials have received considerable attention as a negative electrode for lithium ion secondary batteries. In this study, nano-sized SnO_2-B_2O_3-P_2O_5 particles were synthesized by an Aerosol Flame Deposition(AFD) technique. Single or multi-component amorphous oxide nano particles (soot) were synthesized by supplying metal halide sources such as chloride in the form of gas into an oxy-hydrogen flame. The fine powder obtained was a mixture of crystalline tin oxide and an amorphous phase of B_2O_3 and P_2O_5, resulting in a highly dispersed structure with nano-scale interfaces. According to the XRD results, the as-prepared materials seemed to have a semi-amorphous structure and SEM images showed that the average particle size $<$60 nm. In this study, we investigated the relationship between the structural modification of the tin-based composite oxide and the conductivity as a function of the composition.

Key words: SnO_2-B_2O_3-P_2O_5, Li-ion battery, Aerosol Flame Deposition, Anode materials.

Introduction

Rechargeable lithium ion batteries are considered the most suitable power sources for mobile electronic products such as micro-electro-mechanical systems, smart cards, micro robots, MEMS and medical appliances, etc. An improvement in the capacity and cycle ability of Li-ion batteries in required. Important researches are focused on improved cycle life, high capacity and methods of synthesis. Several materials have been suggested as candidates for the anode. Due to its intense reactivity in air, Li metal is unlikely to become a popular anode material. Also, graphite seems to be impractical as an anode since a proper deposition method is not available. The practical materials for thin film anodes seem to be limited to a metallic alloy of Si [1], amorphous oxides containing Sn [2,3], SnO_2 [4] and some oxynitrides [5].

A conventional anode material based on carbonaceous compounds is usually used, but recently by Fuji photo Film Co. have suggested an amorphous tin-based composite oxide as an anode material [6]. The advantages of tin-based oxide materials are greater specific capacity and higher density compared to graphite so that cells of higher specific energy can be built since tin can reversibly accommodate a maximum of 4.4 lithium atoms per tin atom, in the $Li_{22}Sn_5$ phase. Indeed, the tin composite oxide anode has a capacity nearly twice that of carbon-based negative electrode. This gives a theoretical specific charge capacity of 994 $mAhg^{-1}$, which is much higher than 372 $mAhg^{-1}$ of the fully-lithiated graphite (LiC_6). Due to the substan- tially higher density of tin oxide the volumetric capacity is even more favorable than graphite. Tin oxides are thought to have a two step reaction with lithium:

$$4Li^+ + SnO_2 + 4e^- \rightarrow Sn + 2Li_2O \quad (1)$$

$$xLi^+ + Sn + xe^- \rightarrow Li_xSn(0 \leq x \leq 4.4) \quad (2)$$

The first step involves the irreversible reduction of the tin oxide to tin metal particles in a lithium oxide matrix. The second step is the reversible alloying of the Li^+ into the tin metal. For tin metal, this alloying causes a large volume expansion, causing cracking and crumbling of the material and eventual loss of capacity.

Tin oxide films have been prepared by various methods such as sputtering [7], a spray method [8], chemical vapor deposition [9], electron-beam evaporation [10] and a sol-gel method [11]. Unlike these film preparation techniques, the AFD (Aerosol Flame Deposition) process is unique since it offers a route to prepare nano-porous films composed of nano-sized particles. In this study we have synthesized tin-based composite amorphous oxide (SnO_2-P_2O_5-B_2O_3) by an Aerosol Flame Deposition method and the obtained tin based amorphous composite oxides obtained were tested for electrochemical characteristics to verify the possibility of application in a lithium-ion battery.

Experiments

The precursor solution of tin was prepared by dissolving

*Corresponding author:
Tel : + 82-2-2220-0503
Fax: + 82-2-2299-3851
E-mail: dwshin@hanyang.ac.kr

tin (IV) chloride (Aldrich, 99%) in ethanol at a concentration of 0.05 mol and 0.1 mol. Droplet of tin from a nebulizer with an ultrasonic resonator (1.7 MHz) was subsequently carried into a flame made with conditions of the oxygen flow rate of 7.5 L/minute, Ar shield flow rate of 3 L/minute, and hydrogen flow rate of 1.5 L/minute. The AFD method was applied to fabricate anode films of tin-based amorphous oxide using the system shown in Fig. 1. In the AFD process, a liquid precursor solution was prepared by dissolving the desired precursors into a solvent which was then atomized into micro-sized droplets by an ultrasonic nebulizer. The atomized droplets were carried by Ar carrier gas into a flame hydrolysis reaction in an oxy-hydrogen torch. The vapor of $POCl_3$ and BCl_3 produced by Ar bubbling at a controlled temperature was delivered to an oxy-hydrogen torch and hydrolyzed to form porous oxide soot on Pt substrates**.** The flow rates of source gases were 10, 15, and 20 sccm (BCl_3) and 20, 25, 30 sccm ($POCl_3$) respectively. The notations for the prepared specimen are the abbreviations of the flow rates of these source gases for glass formers. For example, B10P20 denotes a specimen prepared at a flow rate of 10 sccm of BCl_3 and 20sccm of $POCl_3$.

The essential part of the system is the oxy-hydrogen torch, which is made from five concentric tubes creating four concentric gaps, and one shield tube keeping the flame stable. The precursor solution flows through the center most tube of the torch while hydrogen, argon and oxygen flow through four gaps having different widths to ensure laminar flow of the supplied gases. To make uniform depositions, tin-based oxide soot was first deposited on a substrate placed on a rotating stage, which was kept at 150°C to eliminate H_2O and chlorine gas produced during hydrolysis. The whole processes were carried out under a normal air atmosphere with only optional control for moisture. And then, the deposited soot was annealed at 550°C for 10minute in a micro-wave furnace oven. The structural and morphological changes were characterized using X-ray diffractormeter (XRD) by a Rigaku D/max-2500, with CuK_a X-ray radiation 40 mA 100 mV with a scanning step of 0.014 degree and an angular range from 10 to 80 degrees. Specimen surface images of as-deposited and sintered powder were taken using a scanning electron micro-scope (JEOL, JSM-6330F).

To measure the ionic conductivities the amorphous state of tin-based anodes were painted with silver paste on both sides of the specimen as ion blocking electrodes. The electrode area was $1.26 \times 10^{-3}cm^2$ and film height was 6 μm. Conductivity was measured by a complex impedance method using a Solartron 1260 impedance analyzer at various temperatures.

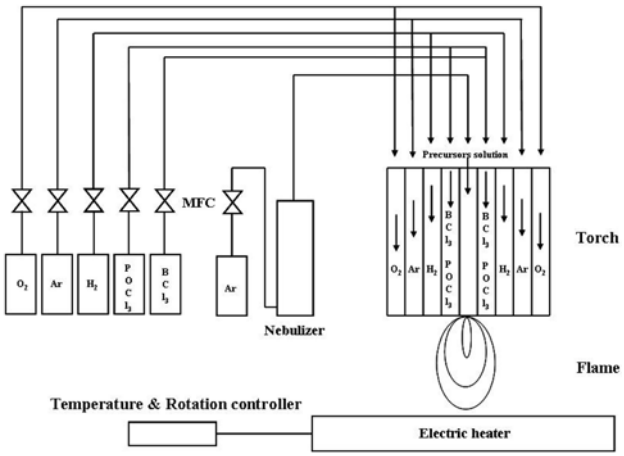

Fig. 1. Schematic diagram of Aerosol Flame Deposition system for the synthesis of tin borophosphate oxide.

Results and discussion

Fig. 2 gives XRD patterns from concentration Sn solution of 0.05 mol and Sn solution of 0.1mol doped boron and phosphorus, tin-based composite oxide powders synthesized at various flow rates of BCl_3 and $POCl_3$. In the case, the Sn solution of 0.05 mol, the synthesized soot was a gray powder. Un doped boron and phosphorus are white powders. This showed that the major peaks of the synthesized white powders fit well to that of crystalline SnO_2 (JCPDS 88-0287). Using a similar synthesis method, white color powder is SnO_2 and gray or yellow powder is Sn metal or SnO [12]. The amorphous background increased with an increase in the flow rate of BCl_3 and $POCl_3$, which is attributed to the formation of the amorphous phase of

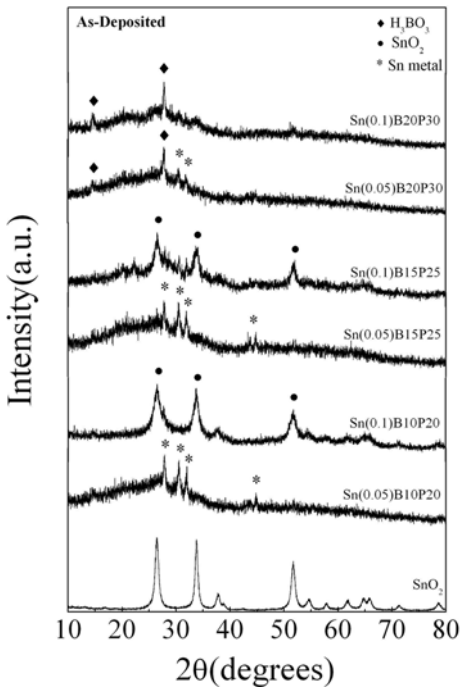

Fig. 2. X-ray diffraction patterns of the SnO_2, SnO_2-B_2O_3-P_2O_5 synthesized powders 0.05 mol% Sn and 0.1 mol% Sn at various flow rates of BCl_3 and $POCl_3$.

B_2O_3 and P_2O_5 and the crystalline H_3BO_3 (JCPDS 30-0199) appeared ($2\theta = 27\text{-}28^o$) due to the reaction with moisture within the oxy-hydrogen flame or atmosphere. However, this phase was eventually converted into B_2O_3 glass former during the heat treatment. XRD patterns of synthesized soot from the Sn solution of 0.1 mol, in contrast with the Sn solution of 0.05 mol, these samples appeared as SnO_2 patterns despite the increase of boron and phosphorus. Because of the growth of Sn and SnO_2 particles synthesized as aerosol methods it has been reported that these are determined by the temperature of the flame during evaporation of solvent [12]. Ionized metals evaporated from an aqueous Sn solution gave Brownian coagulation or were converted into oxide. In our study the crystalline peak of Sn was observed from the Sn solution of 0.05 mol while SnO_2 was observed at 0.1 mol concentration of aqueous Sn. It is estimated that the growth of Sn and SnO_2 particles can be determined by the evaporation time of the solvent. The droplets of an aqueous of 0.05 mol concentration were rapidly evaporated and coagulated into Sn particles. By contrast, the droplets of 0.1 mol concentration need a longer time to evaporate, which converts them to oxide particles from the by oxygen in the touch. B_2O_3 and P_2O_5 are well known as glass network forming compounds. Therefore, the synthesized anode material of a mixture of SnO_2 was expected to be an electronic conductor, and the glass network forming compounds, an ionic conductor.

Fig. 3 gives SEM images of the synthesized powders deposited on Pt substrates at various flow rates of BCl_3 and $POCl_3$. This shows that the tin oxide powders prepared have a particle size of 20~50 nm. The other image are the surfaces of tin borophosphate oxide, which shows that B_2O_3 and P_2O_5 particles were well mixed with Sn. Otherwise, the droplets of 0.1 mol concentration showed B_2O_3 and P_2O_5 mixed with SnO_2 particles.

Fig. 4 are XRD patterns of sample after annealing at 550°C for 10minute in microwave oven. A comparison of the corresponding patterns with a Sn solution of 0.05 mol in Fig. 2 reveals that the crystalline peaks of Sn metal changed to SnO_2 by annealing. Also, B_2O_3 and P_2O_5 formed a glass structure. A Sn solution of 0.1 mol showed that increasing the flow rate of BCl_3 and $POCl_3$, crystalline peaks of SnO_2 diminished appreciably, which means that the B_2O_3 and P_2O_5 formed an amorphous state glass network by annealing.

Fig. 5 gives SEM images of synthesized amorphous powder at various flow rates of BCl_3 and $POCl_3$ deposited on Pt wafers after sintering 550°C for 10 minute. In case of B10P20 and B15P25 is very porous films are seen because of the B_2O_3 and P_2O_5, glass former, is

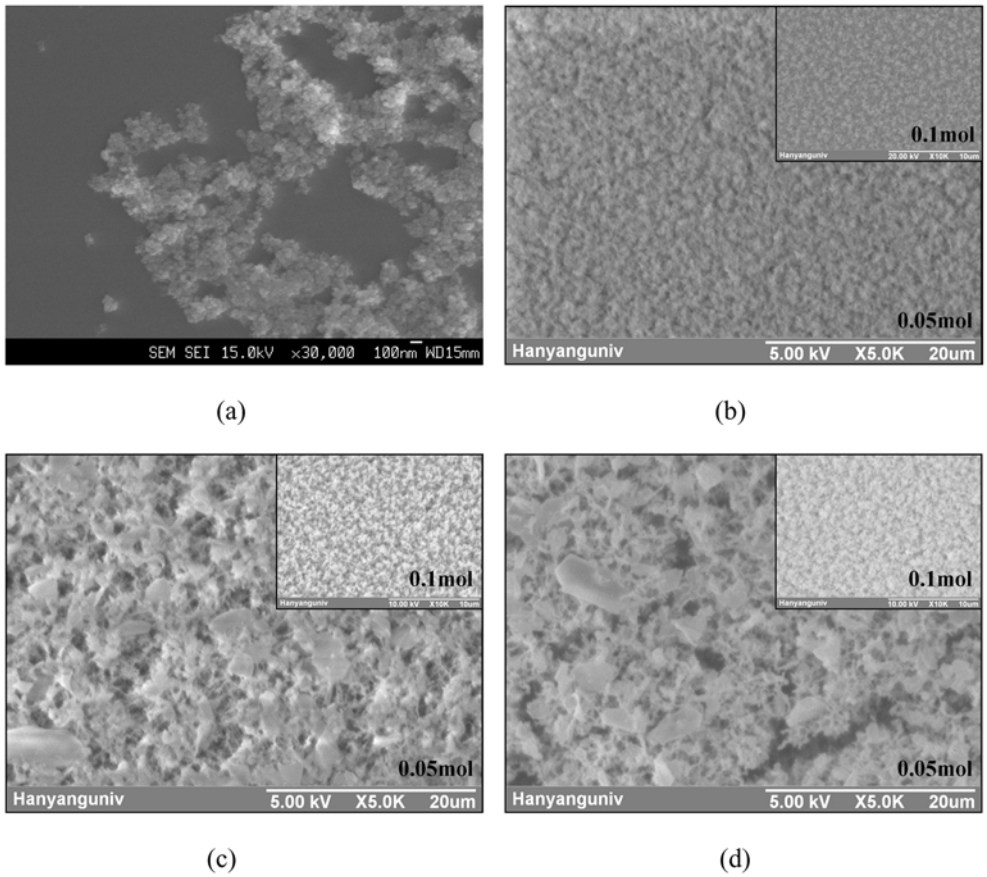

Fig. 3. SEM images of (a) Tin oxide, (b) Sn-B10P20, (c) Sn-B15P25, (d) Sn-B20P30 deposited on Pt wafers.

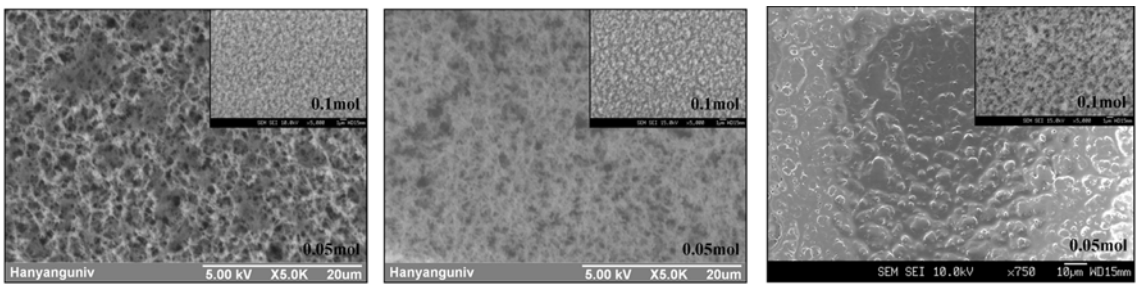

Fig. 5. SEM images of (a) B10P20, (b) B15P25, (c) B20P30 deposited on Pt wafers after sintering at 550°C for 10 minute. (The grey part in the middle of the image due to over-exposure of electron beam).

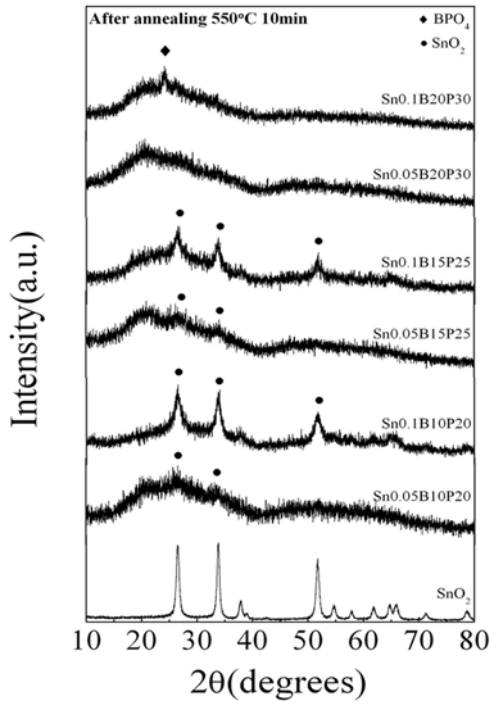

Fig. 4. X-ray diffraction patterns of the synthesized powders 0.05 mol% Sn and 0.1 mol% Sn at various flow rates of BCl_3 and $POCl_3$ after sintering at 550°C for 10 minute.

melted and then evaporated by sintering. In the case of B20P30, a good glass formed state is seen with amorphous state tin oxide doped B_2O_3 and P_2O_5. In the case of 0.1 mol concentration a glass was formed with a porous structure. The amount of B_2O_3 and P_2O_5, glass former, is smaller than in the 0.05 mol case. So it does not form a dense glass. We selected the B20P30 sample for conductivity tests as a function of temperature.

The transition metal oxides are known as ionic and electronic conductors. Because the ionic conductivity depends on temperature, the ionic conductivity is appreciable only at high temperature. Fig. 6 gives an impedance plot measured at various temperatures and an arrhenius plot of B20P30 sample. Although ionic and electronic conductivity were mixed at low temperature, the conductivity of B20P30 sample depended on electronic conductivity of transition metal oxide:

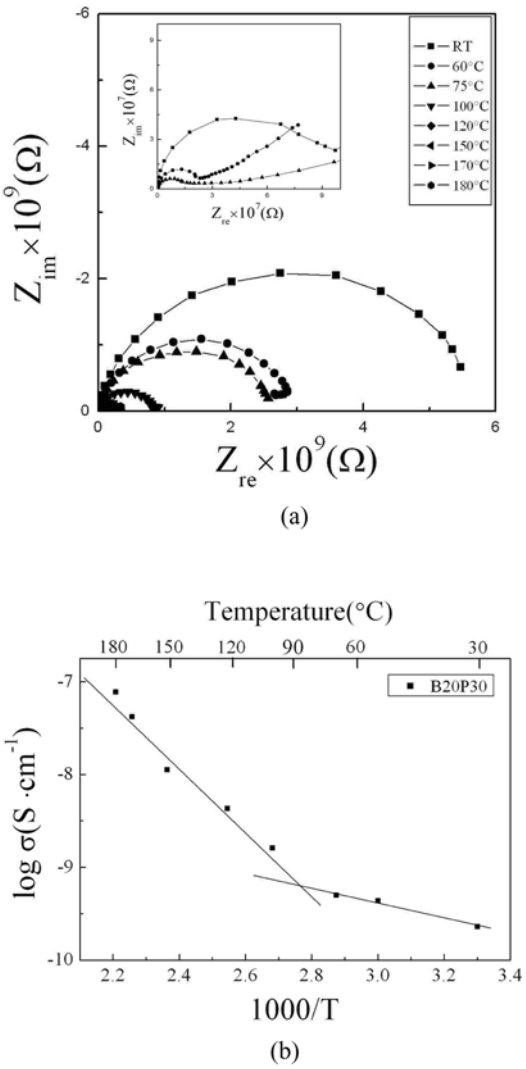

Fig. 6. (a) Typical example of impedance spectra of the B20P30 sample. (b) Electrical conductivity of the B20P30 composite as a function of the inverse of temperature.

$$1n\sigma = 1n\sigma_0 - 1nT + \left(-\frac{E_\alpha}{1000K}\right)\frac{1000}{T} \quad (3)$$

With increasing temperature the conductivity of B20P30 was dominated by ionic conductivity. The impedance plot measured at 150°C is shown as a semi-

circle from ionic conductivity. The activation energy of ionic conductivity was 29.533 J/mol · K or 0.65 eV.

Conclusions

In this study we synthesized tin-based amorphous oxide for thin-film Li-ion secondary batteries by an AFD process. The deposited powders were formed with a porous structure, however the sample of 0.05 mol Sn concentration with B20P30 after annealing 550°C for 10minute formed a dense thin film. Also ionic and electronic conductivity were mixed at a low temperature, however the ionic conductivity is appreciable above 150°C due to SnO_2. The activation energy of B20P30 sample was 68 KJ/mol or 0.65 eV.

Acknowledgements

This work was supported by the Ministry of Information & Communications, Korea, under the Information Technology Research Center (ITRC) Support Program.

References

1. Z. P. Guo, Z. W. Zhao, H. K. Liu and S. X. Dou, J. Power Sources 146 (2005) 190-194.
2. C. Branci, N. Benjelloun, J. Sarradin and M. Ribes, Solid State Ionics 135 (2000) 169-174.
3. M. Mohamedi, S. J. Lee, D. Takahashi, M. Nishizawa, T. Itoh and I. Uchida, Electrochimica Acta 46 (2001) 1161-1168.
4. S. C. Nam, Y. H. Kim, W. I. Cho, B. W. Cho, H. S, Chun and K. S. Yun, Electrochem. 2 (1999) 9-11.
5. B. J. Neudecker, R. A. Zuhr and J. B. Bates, J. Power Sources 81 (1999) 27-32.
6. Y. Idota, T. Kubota, A. Matsufuji, Y. Maekawa and T. Miyasaka, Science 276 (1997) 1395-1397.
7. W. H. Lee, H. C. Son, H. S. Moon, Y. I. Kim, S. H. Sung, J. Y. Kim, J. G. Lee and J. W. Park, J. Power Sources 89 (2000) 102-105.
8. H. Huang, E. M. Kelder, L. Chen and J. Schoonman, J. Power Sources 81 (1999) 362-367.
9. T. Brousse, R. Retoux, U. Herterich and D. M. Schleich, J. Electrochem. Soc. 145 (1998).
10. S. C. Nam, C. H. Paik, W. I. Cho, B. W. Cho, H. S. Chun and K. S. Yun, J. Power Sources 84 (1999) 24-31.
11. J. Santos-pena, T. Brousse, L. Sanchez, J. Morales and D. M. Schleich, J. Power Sources 97 (2001) 232-234.
12. D. H. Hall, A. A. Wang, K. T. Joy, T. A. Miller and M. S. Wooldridge, J. Am. Ceram. Soc., 87 (2004) 2033-2041.